Aalborg Universitet

Optimized Energy Control Scheme for Electric Drive of EV Powertrain Using Genetic Algorithms

Ali, Seyd Muhammad Nawazish; Sharma, Vivek; Hossain, Md. Jahangir; Mukhopadhyay, Subhas; Wang, Dong

Optimized Energy Control Scheme for Electric Drive of EV Powertrain Using Genetic Algorithms

S. M. Nawazish Ali [1,*,†,‡] , **Vivek Sharma** [1,‡] , **M. J. Hossain** [2,‡] , **Subhas C. Mukhopadhyay** [1,‡]
and Dong Wang [3,‡]

1   School of Engineering, Macquarie University, Sydney, NSW 2109, Australia;
    vivek.sharma2@hdr.mq.edu.au (V.S.); subhas.mukhopadhyay@mq.edu.au (S.C.M.)
2   School of Electrical and Data Engineering, University of Technology Sydney, Ultimo, NSW 2007, Australia;
    jahangir.hossain@uts.edu.au
3   Department of Energy Technology, Aalborg University, DK-9220 Aalborg, Denmark; dwa@et.aau.dk
*   Correspondence: syed-muhammad-nawazish.ali@hdr.mq.edu.au
†   Current address: School of Engineering, Macquarie University, Sydney, NSW 2109, Australia.
‡   These authors contributed equally to this work.

Abstract: Automotive applications often experience conflicting-objective optimization problems focusing on performance parameters that are catered through precisely developed cost functions. Two such conflicting objectives which substantially affect the working of traction machine drive are maximizing its speed performance and minimizing its energy consumption. In case of an electric vehicle (EV) powertrain, drive energy is bounded by battery dynamics (charging and capacity) which depend on the consumption of drive voltage and current caused by driving cycle schedules, traffic state, EV loading, and drive temperature. In other words, battery consumption of an EV depends upon its drive energy consumption. A conventional control technique improves the speed performance of EV at the cost of its drive energy consumption. However, the proposed optimized energy control (OEC) scheme optimizes this energy consumption by using robust linear parameter varying (LPV) control tuned by genetic algorithms which significantly improves the EV powertrain performance. The analysis of OEC scheme is conducted on the developed vehicle simulator through MATLAB/Simulink based simulations as well as on an induction machine drive platform. The accuracy of the proposed OEC is quantitatively assessed to be 99.3% regarding speed performance which is elaborated by the drive speed, voltage, and current results against standard driving cycles.

Keywords: induction machine drive; drive energy consumption; linear parameter varying control; EV powertrain; genetic algorithms

1. Introduction

Environmental pollution caused by excessive greenhouse gas emissions, global warming, acid rains and limited reserves have evolved a global energy crisis. One of its significant causes is the continuous use of combustion engine-based vehicles that not only pollute the environment but also result in excessive consumption of oil. An ideal solution in the transportation sector to tackle these challenges is the production of electric vehicles on a massive scale [1]. The core component of an electric vehicle (EV) is its electric motor as it replaces the combustion engine. Induction motors have a sound repute in EV powertrains because of their fascinating technical specifications such as lower requirement for maintenance, de-excitation for inverter fault, and wide speed operation [2].

Some notable examples of these motors in an automotive context are Toyota RAV4 EV (2012), Tesla Model (2012), Honda EV (2012), BMW/X5 (Germany), Chevrolet (USA), Durango (USA), and Renault/Kangoo (1998) [3]. During operation, the induction motor drive in the EV powertrain experiences sheer uncertainties in its parameters particularly due to temperature variations, EV loading, and traffic situations that cause a significant

increase in the demand of voltage and current resulting in excessive battery consumption. The insulation life of a motor's stator winding reduces by half, even with a 10 °C increase beyond thermal limit [4]. Performance optimization of a motor can be achieved either by changing its physical architecture or by developing robust controllers for which different control schemes have been implemented [5].

Field-oriented control (FOC) is normally preferred for drive control of induction motor based EV powertrain but since it uses a proportional-integral (PI) controller, it causes more drive energy consumption because of parameters variation issue [6]. Green energy vehicles using sliding mode control (SMC) to cater parameters variation are presented in [7] but this control approach suffers from chattering, which degrades the drive performance by increasing the energy consumption. A complex solution of this problem is the implementation of higher order SMC given in [8]. A nonlinear sensorless control for induction motor is presented in [9,10] though the work is not in the context of electric vehicles. On the contrary, some notable contributions in the field of drive control applications address the inherent dynamics based linear parameter varying (LPV) control theory [11].

LPV technique is implemented to control only the uncertainties in rotor resistance and load torque of an induction motor in [12]. Only 20% variation in the rotor resistance of induction motor is permitted through LPV framework in [13]. An LPV control scheme for induction machine is utilized in [14] but the only varying parameter is its shaft angle. Induction machine's frequency and rotor resistance variation is addressed in [15] through LPV methodology. Rotor resistance alone is considered as a frozen parameter of induction motor for LPV control design in [16]. A quasi-LPV strategy is adopted for induction machine control in [17]. An amalgam of model reference adaptive system (MRAS) observer with robust LPV scheme is implemented to address only the rotor parameters uncertainity [18]. The variation in the stator variables of induction motor based LPV system is catered through an interval state observer in [19].

LPV control design scheme involves an inevitable, challenging task of weighting functions selection, which is commonly achieved through the method of trial and error [20]. To achieve weighting functions optimization, genetic algorithms are developed. These algorithms originate from stochastic searching stimulated by a natural variety of species and manipulate optimal results for discontinuous problems by genetic formation [21]. These algorithms are implemented in control systems to address the conflicting controller objectives [22]. Here, these objectives are maximizing the drive speed performance and minimizing its energy consumption.

Authors have recently addressed several induction machine drive issues [23,24] with a focus on EV powertrain in LPV frame work [25–27]. The LPV-based scientific contributions discussed earlier are not in the framework of EV applications. As per the author's knowledge, the genetic algorithm-optimized LPV-based control scheme has not been applied in the literature to address the conflicting objectives of reduced drive energy consumption and improved vehicle speed performance for an EV powertrain. Hence, there is a necessity for designing and implementing such an optimized energy control scheme that excellently addresses these significant machine drive objectives against standard driving cycles with a wide range of parameter uncertainties to improve the performance capability of EV powertrain.

The rest of this paper is classified as follows. Section 2 provides the induction machine and LPV system dynamics. Section 3 elaborates the design steps involved in the optimized energy control scheme for induction motor drive of an EV powertrain. Section 4 provides the performance analysis of the proposed energy control scheme through a MATLAB-based vehicle simulator. Section 5 presents the experimental verification on an NI my RIO 1900 control based electric drive platform and overall discussion about the simulation as well as experimental analysis. Section 6 provides the conclusion and highlights the future work.

2. Electric Machine and Control Dynamics

2.1. Induction Motor Dynamics

The dynamics of induction motor in $(\alpha - \beta)$ frame are given as [12]:

$$\dot{\omega}_R = n_P \delta_3 \delta_5 (\phi_{\alpha R} i_{\beta S} - \phi_{\beta R} i_{\alpha S}) - \delta_5 B \omega_R - \delta_5 \tau_L \tag{1}$$

$$\dot{i}_{\alpha S} = -\delta_1 i_{\alpha S} + \delta_2 \phi_{\alpha R} + n_P \delta_3 \delta_6 \phi_{\beta R} \omega_R + \delta_6 V_{\alpha S} \tag{2}$$

$$\dot{i}_{\beta S} = -\delta_1 i_{\beta S} + \delta_2 \phi_{\beta R} - n_P \delta_3 \delta_6 \phi_{\alpha R} \omega_R + \delta_6 V_{\beta S} \tag{3}$$

$$\dot{\phi}_{\alpha R} = -\delta_4 \phi_{\alpha R} - n_P \phi_{\beta R} \omega_R + \delta_3 r_R i_{\alpha S} \tag{4}$$

$$\dot{\phi}_{\beta R} = -\delta_4 \phi_{\beta R} - n_P \phi_{\alpha R} \omega_R + \delta_3 r_R i_{\beta S} \tag{5}$$

where $\sigma = 1 - \frac{L_M^2}{L_S L_R}$, $\delta_1 = \frac{(L_M^2 r_R + L_R^2 r_S)}{\sigma L_S L_R^2}$, $\delta_2 = \frac{L_M r_R}{\sigma L_S L_R^2}$, $\delta_3 = \frac{L_M}{L_R}$, $\delta_4 = \frac{r_R}{L_R}$, $\delta_5 = \frac{1}{J}$, $\delta_6 = \frac{1}{\sigma L_S}$, τ_L represents the load torque, $\phi_{\alpha R}$ and $\phi_{\beta R}$ represent the rotor fluxes, $i_{\alpha S}$ and $i_{\beta S}$ are the stator currents, $V_{\alpha S}$ and $V_{\beta S}$ are the stator voltages. The details of motor parameters used in Equations (1)–(5) are provided in Table 1.

Table 1. Motor parameters.

Symbol	Parameter
n_P	number of pole-pairs
B	damping coefficient
L_M	magnetizing inductance
L_S	stator self-inductance
L_R	rotor self-inductance
J	moment of inertia
r_R	rotor resistance
r_S	stator resistance

2.2. LPV System Dynamics

The induction motor dynamics are transformed into LPV system dynamics by considering r_R and r_S as the time varying parameters. The new system in its state space form is given as follows:

$$\mathbf{G}(\chi(t)) : \dot{x} = \mathbf{A}(\chi(t))x + \mathbf{B}(\chi(t))u$$

$$y = \mathbf{C}(\chi(t))x + \mathbf{D}(\chi(t))u \tag{6}$$

where $x(t) = [i_{\alpha S} \ i_{\beta S} \ \phi_{\alpha R} \ \phi_{\beta R}]^T$, $\chi(t) = [\chi_1 \ \chi_2]^T = [r_R(t) \ r_S(t)]^T$ is the time varying parameter, $y(t) = [i_{\alpha S} \ i_{\beta S}]^T$ and $u(t) = [V_{\alpha S} \ V_{\beta S}]^T$. The LPV model-based system matrix of induction motor is as follows:

$$\mathbf{A}(\chi(t)) = \begin{bmatrix} -\left(\frac{\chi_2}{\kappa} + \frac{\chi_1 L_M^2}{\kappa L_R^2}\right) & 0 & \frac{\chi_1 L_M}{\kappa L_R^2} & \frac{n_P \omega_R L_M}{\kappa L_R} \\ 0 & -\left(\frac{\chi_2}{\kappa} + \frac{\chi_1 L_M^2}{\kappa L_R^2}\right) & -\frac{n_P \omega_R L_M}{\kappa L_R} & \frac{\chi_1 L_M}{\kappa L_R^2} \\ \frac{\chi_1 L_M}{L_R} & 0 & -\frac{\chi_1}{L_R} & -n_P \omega_R \\ 0 & \frac{\chi_1 L_M}{L_R} & n_P \omega_R & -\frac{\chi_1}{L_R} \end{bmatrix}$$

$$\mathbf{B} = \begin{bmatrix} \frac{1}{\kappa} & 0 \\ 0 & \frac{1}{\kappa} \\ 0 & 0 \\ 0 & 0 \end{bmatrix}, \mathbf{C} = \begin{bmatrix} 1 & 0 & 0 & 0 \\ 0 & 1 & 0 & 0 \end{bmatrix}, \mathbf{D} = \begin{bmatrix} 0 & 0 \\ 0 & 0 \end{bmatrix} \tag{7}$$

where $\kappa = \sigma L_S$.

3. Optimized Energy Control Scheme

The LPV-based optimized energy control scheme tuned through the genetic algorithms is presented in Figure 1 and explained in detail by the following stepwise procedure:
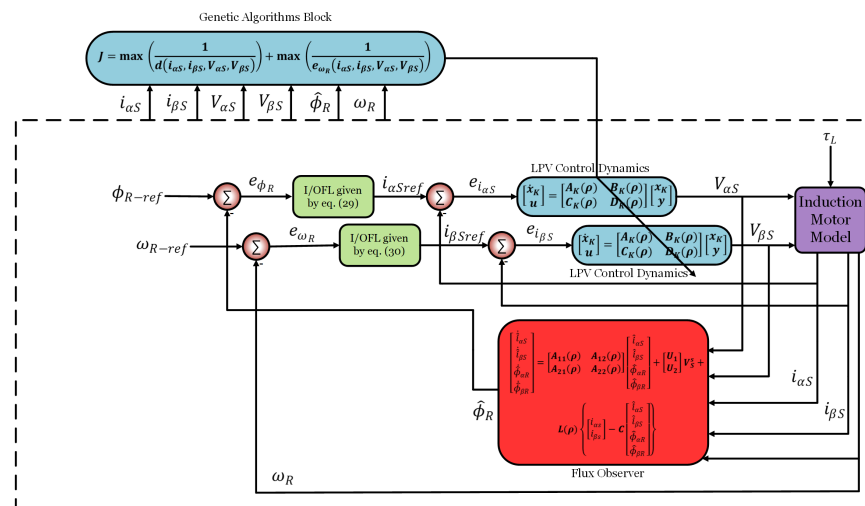

Figure 1. Optimized energy control scheme.

3.1. Cost Function Synthesis

In order to deal with the conflicting but significant objectives of various engineering applications, appropriate formulation of cost functions is necessary. Here, these objectives are:

1. Maximizing the speed performance of electric drive of EV powertrain;
2. Minimizing the energy consumption of electric drive of EV powertrain.

A cost function addressing these objectives with in the overall control design is formulated as follows:

$$J = max \left(\frac{1}{d(i_{\alpha S}, i_{\beta S}, V_{\alpha S}, V_{\beta S})} \right) + max \left(\frac{1}{e_{\omega_R}(i_{\alpha S}, i_{\beta S}, V_{\alpha S}, V_{\beta S})} \right) \tag{8}$$

where d and e_{ω_R} represent the drive energy consumption and speed performance error, respectively.

3.2. Observer Synthesis

A robust observer is formulated for the accurate flux estimation. The mathematical flow of this observer is presented as [12]:

$$\hat{\mathbf{G}}\chi(t) : \frac{d}{dt}\hat{x} = \mathbf{A}\chi(t)\hat{x} + \mathbf{B}u + \mathbf{L}(\chi)\left\{ \mathbf{i_S^s} - \mathbf{C}\begin{bmatrix} \mathbf{i_S^s} \\ \phi_R^s \end{bmatrix} \right\} \tag{9}$$

$$
\begin{bmatrix} \dot{\hat{i}}_{\alpha S} \\ \dot{\hat{i}}_{\beta S} \\ \dot{\hat{\phi}}_{\alpha R} \\ \dot{\hat{\phi}}_{\beta R} \end{bmatrix} = \begin{bmatrix} \mathbf{A_{11}}(\chi) & \mathbf{A_{12}}(\chi) \\ \mathbf{A_{21}}(\chi) & \mathbf{A_{22}}(\chi) \end{bmatrix} \begin{bmatrix} \hat{i}_{\alpha S} \\ \hat{i}_{\beta S} \\ \hat{\phi}_{\alpha R} \\ \hat{\phi}_{\beta R} \end{bmatrix} + \begin{bmatrix} \mathbf{U_1} \\ \mathbf{U_2} \end{bmatrix} \begin{bmatrix} V_{\alpha S} \\ V_{\beta S} \end{bmatrix} + \mathbf{L}(\chi) \left\{ \begin{bmatrix} i_{\alpha S} \\ i_{\beta S} \end{bmatrix} - \mathbf{C} \begin{bmatrix} \hat{i}_{\alpha S} \\ \hat{i}_{\beta S} \\ \hat{\phi}_{\alpha R} \\ \hat{\phi}_{\beta R} \end{bmatrix} \right\} \tag{10}
$$

where

$$
\mathbf{A_{11}} = \begin{bmatrix} -\delta_1 & 0 \\ 0 & -\delta_1 \end{bmatrix}, \mathbf{A_{12}} = \begin{bmatrix} \delta_2 & n_P \delta_2 \omega_R \\ -n_P \delta_2 \omega_R & \delta_2 \end{bmatrix}
$$

$$
\mathbf{A_{21}} = \begin{bmatrix} \chi_1 \delta_3 & 0 \\ 0 & \chi_1 \delta_3 \end{bmatrix}, \mathbf{A_{22}} = \begin{bmatrix} -\delta_4 & -n_P \omega_R \\ n_P \omega_R & -\delta_4 \end{bmatrix}
$$

$$
\mathbf{U_1} = \begin{bmatrix} \delta_6 & 0 \\ 0 & \delta_6 \end{bmatrix}, \mathbf{U_2} = \begin{bmatrix} 0 & 0 \\ 0 & 0 \end{bmatrix}
$$

$\mathbf{L}(\chi)$ is the observer's gain matrix. Its error equation is formed by rotor fluxes and stator currents as shown below:

$$
\mathbf{e} = \begin{bmatrix} i_{\alpha S} \\ i_{\beta S} \\ \phi_{\alpha R} \\ \phi_{\beta R} \end{bmatrix} - \begin{bmatrix} \hat{i}_{\alpha S} \\ \hat{i}_{\beta S} \\ \hat{\phi}_{\alpha R} \\ \hat{\phi}_{\beta R} \end{bmatrix} \tag{11}
$$

The above equation can be represented in state space form as:

$$
\dot{\mathbf{e}} = \left(\begin{bmatrix} \mathbf{A_{11}}(\chi) & \mathbf{A_{12}}(\chi) \\ \mathbf{A_{21}}(\chi) & \mathbf{A_{22}}(\chi) \end{bmatrix} - \mathbf{L}(\chi)\mathbf{C} \right) \mathbf{e} \tag{12}
$$

3.3. Weighting Gains

The affine matrices, i.e., $\mathbf{A}(\chi)$ (system matrix) and $\mathbf{L}(\chi)$ (observer gain matrix) obtained from Sections 2.2 and 3.2 in the proposed control scheme fulfill the design objectives of tracking, robustness and stability by using H_∞ norm that involves loop shaping. Genetic algorithms have been used to tune these H_∞ sensitivity and weighting gains given in Table 2.

Table 2. Weighting gains.

Gain	Value
Complementary sensitivity ($\mathbf{W_t}$)	$\frac{(0)s+w_T}{(0)s+1}$
Control sensitivity ($\mathbf{W_{ks}}$)	$\frac{c(s+w_{ks})}{M_k(s+cw_{ks})}$ $c = 10^4$
Sensitivity ($\mathbf{W_s}$)	$\frac{(1/M_s)s+w_B}{s+w_B A}$ w_B = bandwidth = 550 A = factor of attenuation = 0.002

where M_k, w_T and M_s are the genetic algorithm-tuned design parameters.

3.4. Optimized Control Unit

To meet the desired conflicting objectives, the closed-loop control develops the required current vector by using the voltage vector in LPV framework. Such a plant (generalized) in its polytopic state space form is given by:

$$\begin{bmatrix} \dot{\mathbf{x}} \\ \mathbf{z} \\ \mathbf{y} \end{bmatrix} = \begin{bmatrix} \mathbf{A}(\chi,\zeta) & \mathbf{B_w}(\chi,\zeta) & \mathbf{B_u}(\zeta) \\ \mathbf{C_z}(\chi,\zeta) & \mathbf{D_{zw}}(\chi,\zeta) & \mathbf{D_{zu}}(\zeta) \\ \mathbf{C_y} & \mathbf{D_{yw}} & 0 \end{bmatrix} \begin{bmatrix} \mathbf{x} \\ \mathbf{w} \\ \mathbf{u} \end{bmatrix} \tag{13}$$

where $\mathbf{z} = [z_s\ z_t\ z_k]^T$ is a vector for control outputs and $\mathbf{w} = [i_{\alpha Sref}\ i_{\beta Sref}]^T$ is a vector for external inputs. The values of $\mathbf{z}$ originate from the weighting gains mentioned in Table 2. The complete structure of this plant is explained in [23]. $\mathbf{A}$, $\mathbf{B_w}$, $\mathbf{B_u}$, $\mathbf{C_z}$, $\mathbf{D_{zw}}$, $\mathbf{D_{zu}}$, $\mathbf{C_y}$, $\mathbf{D_{yw}}$ denote the closed-loop control system matrices, whereas the vector for optimized weighting functions through genetic algorithms is denoted by ζ. χ gives the varying parameter which can also be represented as:

$$\chi(t) = (\chi_1, \chi_2, ..., \chi_N)^T \tag{14}$$

The range for χ_i is pre-defined as:

$$\chi_i(t) \in [\chi_{min}\ \chi_{max}] \tag{15}$$

The extension of $\mathbf{A}(\chi(t))$ is given by:

$$\mathbf{A}(\chi(\mathbf{t})) = \mathbf{A}(r_R, r_S) = \mathbf{A_0} + \chi_1 \mathbf{A_1} + \chi_2 \mathbf{A_2}$$
$$\mathbf{A}(\chi(\mathbf{t})) = \mathbf{A_0} + r_R \mathbf{A_1} + r_S \mathbf{A_2} \tag{16}$$

$\chi(\mathbf{t})$ after convex decomposition becomes:

$$\chi(\mathbf{t}) = \alpha_1 \chi_{11} + \alpha_2 \chi_{12} + \alpha_3 \chi_{21} + \alpha_4 \chi_{22} \tag{17}$$

with

$$\sum_{i=1}^{4} \alpha_i = 1 \ and \ \alpha_i \geq 0$$

where α_i defines the corner of polytopic parameter array whose values are given by:

$$\chi_{11} = (0, r_{Rmin}), \chi_{12} = (0, r_{Rmax})$$
$$\chi_{21} = (0, r_{Smin}), \chi_{22} = (0, r_{Smax}) \tag{18}$$

The motor plant in its polytopic form with vertex value χ is formulated as follows:

$$\mathbf{G}(\chi) = \alpha_1 \mathbf{G}(\chi_{11}) + \alpha_2 \mathbf{G}(\chi_{12}) + \alpha_3 \mathbf{G}(\chi_{21}) + \alpha_4 \mathbf{G}(\chi_{22}) \tag{19}$$

$$\alpha_1 = \frac{r_R(t) - r_{R\,min}}{r_{R\,max} - r_{R\,min}}, \alpha_2 = \frac{r_R(t) - r_{R\,max}}{r_{R\,max} - r_{R\,min}}, \alpha_3 = \frac{r_S(t) - r_{S\,min}}{r_{S\,max} - r_{S\,min}}, \alpha_4 = \frac{r_S(t) - r_{S\,max}}{r_{S\,max} - r_{S\,min}} \tag{20}$$

The dynamics of optimized controller are given by:

$$\begin{bmatrix} \dot{\mathbf{x_K}} \\ \mathbf{u} \end{bmatrix} = \begin{bmatrix} \mathbf{A_K}(\chi) & \mathbf{B_K}(\chi) \\ \mathbf{C_K}(\chi) & \mathbf{D_K}(\chi) \end{bmatrix} \begin{bmatrix} \mathbf{x_K} \\ \mathbf{y} \end{bmatrix} \tag{21}$$

such that it satisfies the inherent stability of the designed feedback control system Equations (13) and (21) and gurantees its induced L_2 norm bounded by $\gamma > 0$. If there exist $\mathbf{Y}(\chi)$ and $\mathbf{Z}(\chi)$ which are symmetric as well as parameter-dependent matrices, whereas $\widetilde{\mathbf{A}}_\mathbf{K}(\chi)$, $\widetilde{\mathbf{B}}_\mathbf{K}(\chi)$, $\widetilde{\mathbf{C}}_\mathbf{K}(\chi)$ and $\widetilde{\mathbf{D}}_\mathbf{K}(\chi)$ are gain matrices, the below mentioned linear matrix inequalities are satisfied [20]:

$$
\begin{bmatrix}
\mathbf{H_{11}}(\chi,\zeta) & \mathbf{H_{12}}(\chi,\zeta) & \mathbf{H_{13}}(\chi,\zeta) & \mathbf{H_{14}}(\chi,\zeta) \\
* & \mathbf{H_{22}}(\chi,\zeta) & \mathbf{H_{23}}(\chi,\zeta) & \mathbf{H_{24}}(\chi,\zeta) \\
* & * & \mathbf{H_{33}}(\chi,\zeta) & \mathbf{H_{34}}(\chi,\zeta) \\
* & * & * & \mathbf{H_{44}}(\chi,\zeta)
\end{bmatrix} < 0
$$

$$
\begin{bmatrix}
\mathbf{Z} & \mathbf{I} \\
\mathbf{I} & \mathbf{Y}
\end{bmatrix} > 0
$$

where

$$
\begin{aligned}
\mathbf{H_{11}}(\chi,\zeta) &= \mathbf{A}(\chi,\zeta)\mathbf{Z} + \mathbf{Z}\mathbf{A}(\chi,\zeta)^T + \mathbf{B_u}\tilde{\mathbf{C}}_{\mathbf{K}}(\chi) \\
&\quad + (\mathbf{B_u}\tilde{\mathbf{C}}_{\mathbf{K}}(\chi))^T \\
\mathbf{H_{12}}(\chi,\zeta) &= \tilde{\mathbf{A}}_{\mathbf{K}}(\chi) + \mathbf{A}(\chi,\zeta) + \mathbf{B_u}\tilde{\mathbf{D}}_{\mathbf{K}}(\chi)\mathbf{C_v} \\
\mathbf{H_{13}}(\chi,\zeta) &= \mathbf{B_w}(\chi,\zeta) + \mathbf{B_u}\tilde{\mathbf{D}}_{\mathbf{K}}(\chi)\mathbf{D_{vw}} \\
\mathbf{H_{14}}(\chi,\zeta) &= (\mathbf{C_z}(\chi,\zeta)\mathbf{Z} + \mathbf{D_{zu}}\tilde{\mathbf{C}}_{\mathbf{K}}(\chi))^T \\
\mathbf{H_{22}}(\chi,\zeta) &= \mathbf{A}(\chi,\zeta)^T\mathbf{Y} + \mathbf{Y}\mathbf{A}(\chi,\zeta) + \tilde{\mathbf{B}}_{\mathbf{K}}(\chi)\mathbf{C_v} \\
&\quad + (\tilde{\mathbf{B}}_{\mathbf{K}}(\chi)\mathbf{C_v})^T \\
\mathbf{H_{23}}(\chi,\zeta) &= \mathbf{Y}\mathbf{B_w}(\chi,\zeta) + \tilde{\mathbf{B}}_{\mathbf{K}}(\chi)\mathbf{D_{vw}} \\
\mathbf{H_{24}}(\chi,\zeta) &= (\mathbf{C_z}(\chi,\zeta) + \mathbf{D_{zu}}\tilde{\mathbf{D}}_{\mathbf{K}}(\chi)\mathbf{C_v})^T \\
\mathbf{H_{33}}(\chi,\zeta) &= -\gamma\mathbf{I} \\
\mathbf{H_{34}}(\chi,\zeta) &= (\mathbf{D_{zw}}(\chi,\zeta) + \mathbf{D_{zu}}\tilde{\mathbf{D}}_{\mathbf{K}}(\chi)\mathbf{D_{vw}})^T \\
\mathbf{H_{44}}(\chi,\zeta) &= -\gamma\mathbf{I}
\end{aligned}
\tag{22}
$$

($*$) denotes symmetry. The objectives of the former and later inequalities are to achieve the optimized attenuation factor (γ) and to satisfy the positive definite condition, respectively. That optimized value comes out to be 0.802. The solution of LMIs generates the gain matrices $\tilde{\mathbf{A}}_{\mathbf{K}}(\chi)$, $\tilde{\mathbf{B}}_{\mathbf{K}}(\chi)$, $\tilde{\mathbf{C}}_{\mathbf{K}}(\chi)$, $\tilde{\mathbf{D}}_{\mathbf{K}}(\chi)$ and symmetric parameter-dependent matrices $\mathbf{Y}(\chi)$ and $\mathbf{Z}(\chi)$. The gains of designed controller $\mathbf{A_K}$, $\mathbf{B_K}$, $\mathbf{C_K}$ and $\mathbf{D_K}$ can be calculated by:

$$
\mathbf{D_K} = \tilde{\mathbf{D}}_{\mathbf{K}}
\tag{23}
$$

$$
\mathbf{C_K} = (\tilde{\mathbf{C}}_{\mathbf{K}} - \mathbf{D_K}\mathbf{C_v}\mathbf{Y})(\mathbf{V}^T)^{-1}
\tag{24}
$$

$$
\mathbf{B_K} = \mathbf{W}^{-1}(\tilde{\mathbf{B}}_{\mathbf{K}} - \mathbf{Z}\mathbf{B_u}\mathbf{D_K})
\tag{25}
$$

$$
\mathbf{A_K} = \mathbf{W}^{-1}(\tilde{\mathbf{A}}_{\mathbf{K}} - \mathbf{W}\mathbf{B_K}\mathbf{C_v}\mathbf{Y} - \mathbf{Z}\mathbf{B_u}\mathbf{C_K}\mathbf{V}^T -
$$
$$
\mathbf{Z}(\mathbf{A} + \mathbf{B_u}\mathbf{D_K}\mathbf{C_v})\mathbf{Y})(\mathbf{W}^T)^{-1}
\tag{26}
$$

where $\mathbf{V}$ and $\mathbf{W}$ are matrices such that

$$
\mathbf{I} - \mathbf{Z}\mathbf{Y} = \mathbf{W}\mathbf{V}^T
\tag{27}
$$

Further simplification gives the following form of the proposed gain scheduling optimized LPV control:

$$
\begin{bmatrix}
\mathbf{A_K}(\chi) & \mathbf{B_K}(\chi) \\
\mathbf{C_K}(\chi) & \mathbf{D_K}(\chi)
\end{bmatrix} = \sum_{i=1}^{4} \alpha_i \begin{bmatrix}
\mathbf{A_K}(\chi_i) & \mathbf{B_K}(\chi_i) \\
\mathbf{C_K}(\chi_i) & \mathbf{D_K}(\chi_i)
\end{bmatrix}
\tag{28}
$$

3.5. Optimization of Weighting Functions

An important real positive scalar that affects the performance objectives in this energy control scheme is γ. That is why it is included in the weighting fuction's decision vector ζ. A flow chart elaborating the steps involved in the controller synthesis through weighting functions optimization is shown in Figure 2.
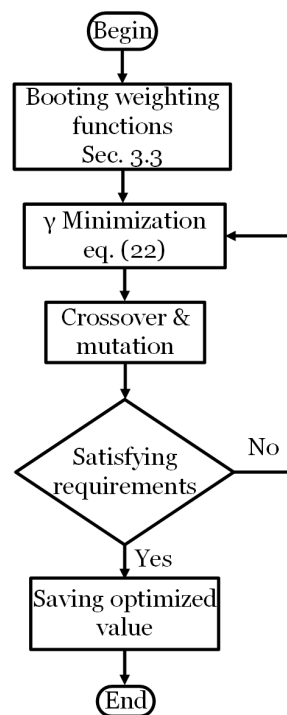
Figure 2. Controller synthesis through genetic algorithms.

3.6. Optimized Flux and Speed Control Unit

For the perfect tracking of drive flux and speed, an input–output feedback linearization (I/OFL) control technique is applied which takes $\mathbf{i_S} = [i_{\alpha S}\ i_{\beta S}]^T$ as input and $\mathbf{y} = [\omega_R\ \phi_R]^T$ as output. The reference currents for the stator are generated by taking derivates of the flux and speed relations accompanied with control regulation through appropriate gains. These currents are:

$$i_{\alpha Sref} = \frac{\hat{\phi}_{\alpha R}}{\delta_3 r_R}\left(\frac{\dot{\hat{\phi}}_R}{\hat{\phi}_R} + \delta_4\right) + \frac{\hat{\phi}_{\beta R}}{n_P^2 \delta_3 \delta_5^2 \hat{\phi}_R^2}\left(-\dot{\omega}_R - \delta_5 \tau_L - \delta_5 B \omega_R\right) \tag{29}$$

$$i_{\beta Sref} = \frac{\hat{\phi}_{\beta R}}{\delta_3 r_R}\left(\frac{\dot{\hat{\phi}}_R}{\hat{\phi}_R} + \delta_4\right) + \frac{\hat{\phi}_{\beta R}}{n_P^2 \delta_3 \delta_5^2 \hat{\phi}_R^2}\left(\dot{\omega}_R + \delta_5 \tau_L + \delta_5 B \omega_R\right) \tag{30}$$

where $\dot{\hat{\phi}}_R$ can be obtained by:

$$-\delta_4 \hat{\phi}_R + \delta_3 r_R \left(\frac{\hat{\phi}_{\alpha R} i_{\alpha S} + \hat{\phi}_{\beta R} i_{\beta S}}{\hat{\phi}_R}\right) \tag{31}$$

The above-mentioned Equations (29) and (30) formulate the tracking errors $e_{\phi_R} = \phi_{R-ref} - \hat{\phi}_R$ and $e_{\omega_R} = \omega_{R-ref} - \omega_R$ for the drive flux and speed, respectively.

4. Performance Analysis of Optimized Energy Control

The effectiveness of the proposed energy control scheme is validated through non-linear MATLAB-based simulations on a developed vehicle simulator against the New European Driving Cycle (NEDC).

4.1. Vehicle Dynamics

An EV simulator is developed as shown in Figure 3 with specifications mentioned in Table 3 [26]. It takes NEDC and Highway Fuel Economy Test (HWFET) driving cycles as desired speed which is then given to the driver section comprising a PI controller. The driver generates the driving command for the electric machine drive which is further

embedded in vehicular dynamics through transmission. The drive energy as well as speed performance of the EV powertrain suffers due to the uncertainty in motor drive parameters caused by driving cycle schedules, traffic state, EV loading, and drive temperature. These factors are taken into account during simulation analysis by considering standard driving cycles at higher temperatures. The temperature values are accomodated by their relation with the resistance values as given by [28]:

$$R = R_0[1 + \alpha \Delta T] \tag{32}$$

where ΔT, α and R_0 represents temperature difference, temperature coefficient and material's resistance, respectively. Mathematical model-based rotor and stator resistance estimation is used to generate a temperature profile throughout the standard driving cycles which contains constant speed, acceleration and deceleration. These resistances are as follows [29,30]:

$$r_R = \sqrt{\omega_{sl}^2 L_R \left[\frac{\omega_e L_M^2}{\frac{Q}{I_S^2} + \omega_e L_S} - L_R \right]} \tag{33}$$

$$r_S = k r_R \tag{34}$$

where ω_e and ω_{sl} are the electrical frequency and slip, respectively. The vehicle dynamics in mathematical form including speed of EV (n_R), load torque of EV ($\tau_{L(EV)}$) and traction force of EV (F_t) are given as follows:

$$n_R = \frac{r_W}{g_R} \omega_R \tag{35}$$

$$\tau_{L(EV)} = \frac{F_t r_W}{g_R} \tag{36}$$

$$F_t = F_g + F_i + F_r + F_a \tag{37}$$

where:
F_i: inertial resistance
F_a: aerodynamic drag
F_g: grade resistance
F_r: rolling resistance
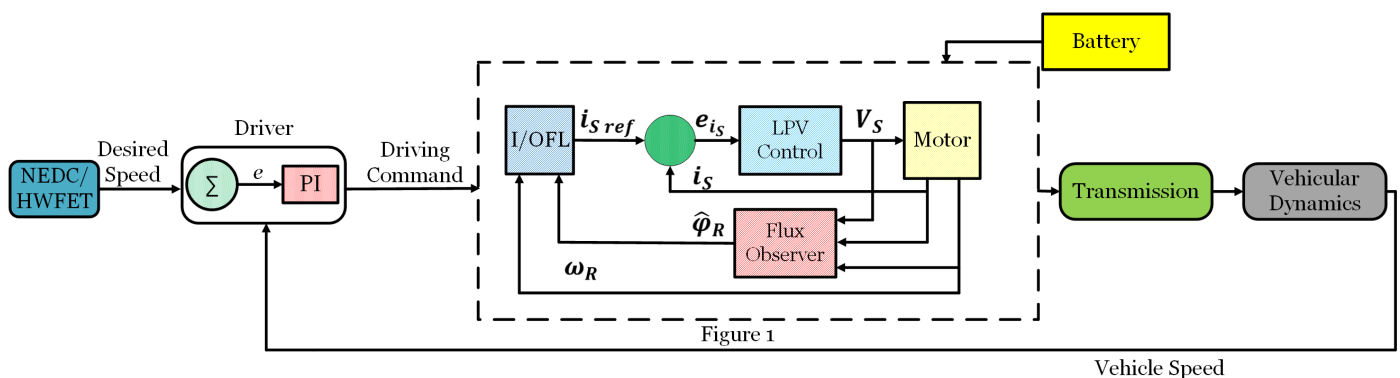r_W: radius of EV wheel
g_R: gear ratio

Figure 3. Electric vehicle control simulator.

Table 3. Specifications of EV.

Symbol	Parameter	Value
m	Mass	1000 kg
C_r	Coefficient of rolling resistance	0.014
A_F	Frontal area	2.1 m^2
C_d	Coefficient of aerodynamic drag	0.4
R_{wheel}	Wheel radius	0.2 m

4.2. Higher Order SMC-Based NEDC Comparison

The efficacy and robustness of the proposed OEC scheme is validated by comparing it with a Higher Order SMC technique given in [31]. To make a precise comparison, the motor parameters are taken from [31], i.e., $J = 0.01$ kg.m^2, $L_M = 377$ mH, $r_S = 14.1$ Ω, $L_S = 400$ mH, $r_R = 10.1$ Ω and $L_R = 412.8$ mH. NEDC is used as speed profile for the electric vehicle control simulator considering an elevated temperature. The comparison of the conflicting objectives of the EV powertrain, i.e., speed tracking performance and drive energy consumption in the form of voltages and currents is shown in Figures 4–7, respectively. Furthermore, the NEDC-based tracking of the motor flux through the designed flux observer of OEC scheme is also shown in Figure 8. As mentioned in [31], a 20–60% change in the rated values of motor resistances is considered. It can be analyzed from the obtained results that OEC scheme provides better speed tracking with less drive energy consumption for EV powertrain than its control counterpart under varying machine parameters.
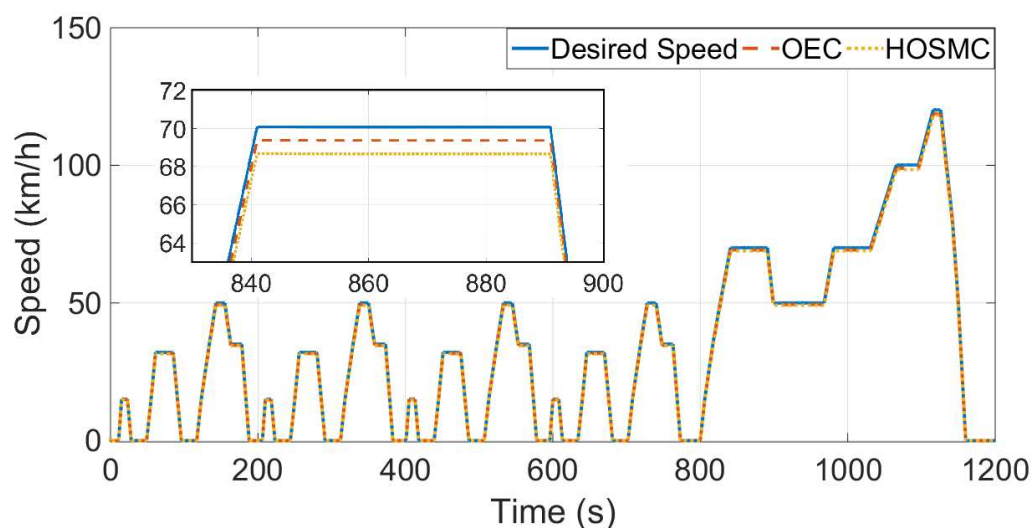
Figure 4. NEDC based analysis at 60 °C.
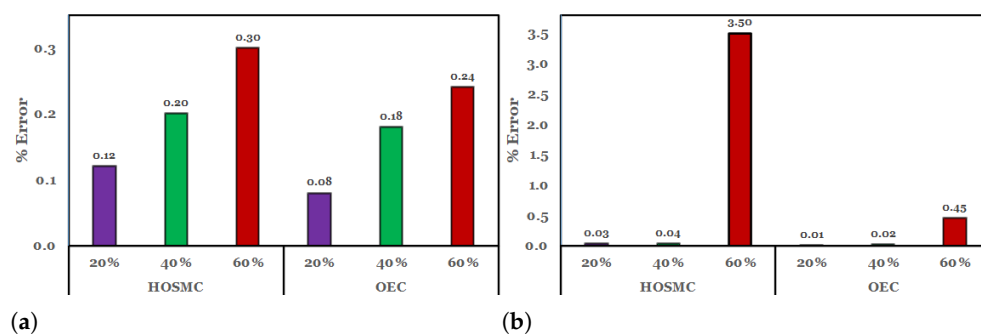
Figure 5. EV Speed tracking performance comparison (**a**) for stator resistance variation (**b**) for rotor resistance variation.
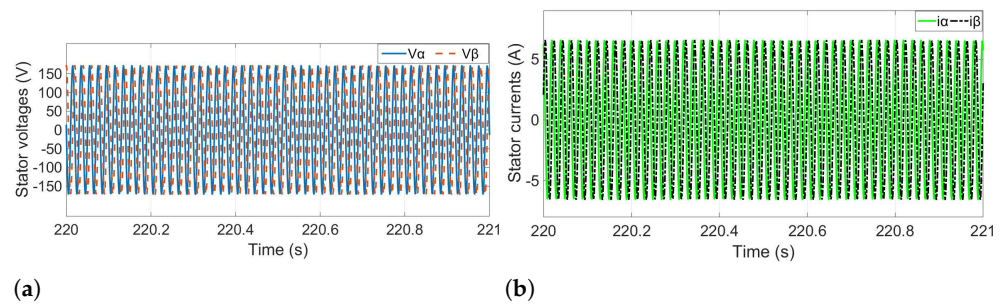
Figure 6. SMC-based EV powertrain (**a**) Voltages (**b**) Currents.
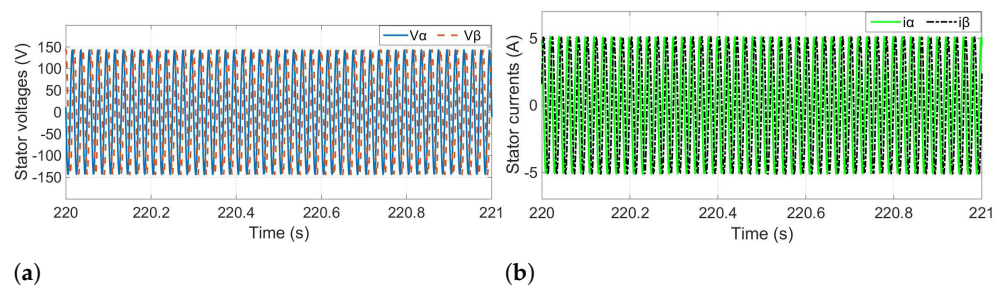

Figure 7. OEC-based EV powertrain (**a**) Voltages (**b**) Currents.
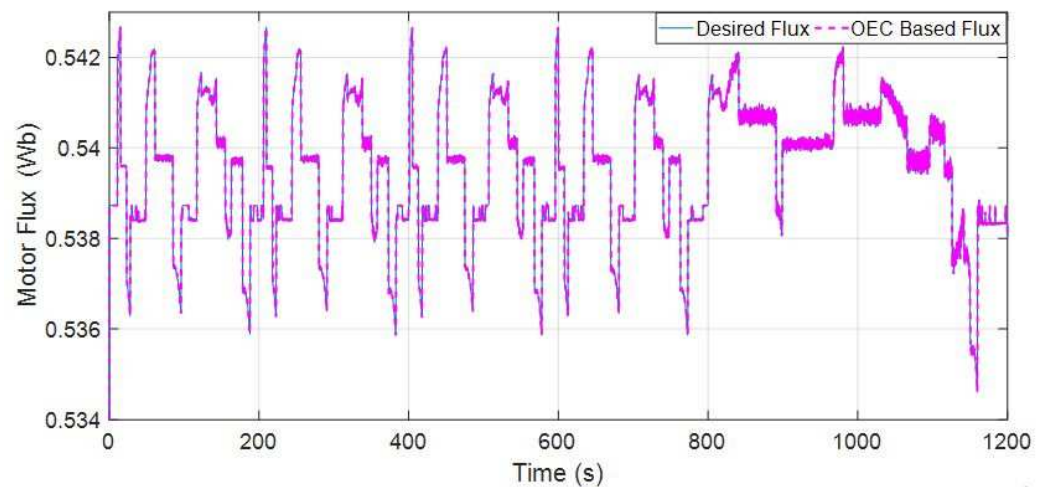

Figure 8. OEC-based flux tracking at 60 °C.

4.3. Higher Order SMC-Based Dynamic Behavior Comparison

The analysis of the proposed control scheme is extended to include the dynamic behavior of the induction motor drive under various circumstances. For that purpose, the above mentioned Higher Order SMC along with the same parameters is compared with the proposed OEC at elevated tenperature with respect to the dynamic characteristics (torque and speed) of drive. The comparison is shown in Figure 9. It can be clearly observed from the figure that even at a higher temperature, the dynamic characteristics of the drive in case of OEC scheme in comparison with Higher Order SMC are quite close to the characteristics at room temperature at which the resistances are at their nominal values. The analysis considers a unipolar load torque which means it has two steady state points (one is for rising edge and other for falling edge). They are also reflecting in the circular portion of the obtained dynamic characteristics.
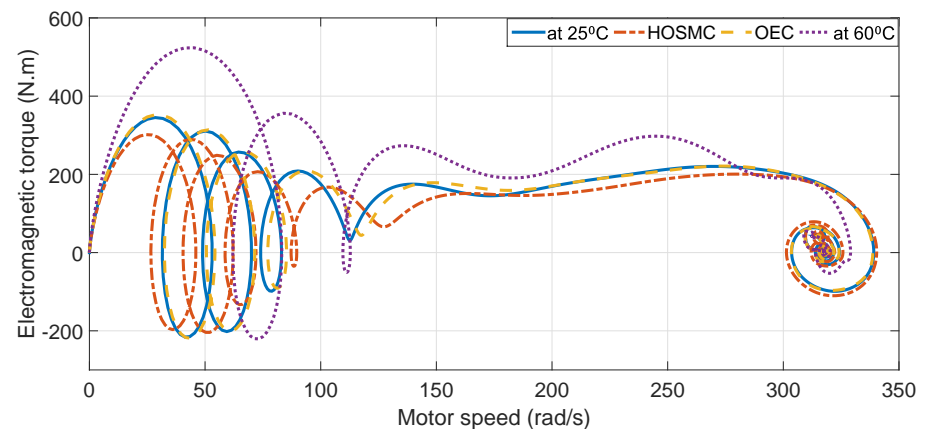
Figure 9. Comparison of motor dynamic behavior.

5. Experimental Analysis

The proposed OEC scheme is also tested on an induction machine drive testing platform as given in Figure 10. It is a 2.2 kW induction motor based setup comprising an inverter, an autotransformer and a controller kit based on NI myRIO 1900 which is further interfaced with a computer. The proposed control algorithm is implemented in it and the microprocessor performs the functions of data logging, downloading and data communication. A DL 1019P and DL 2006E (range of 150N) are used together as magnetic powder brake and load cell, respectively.
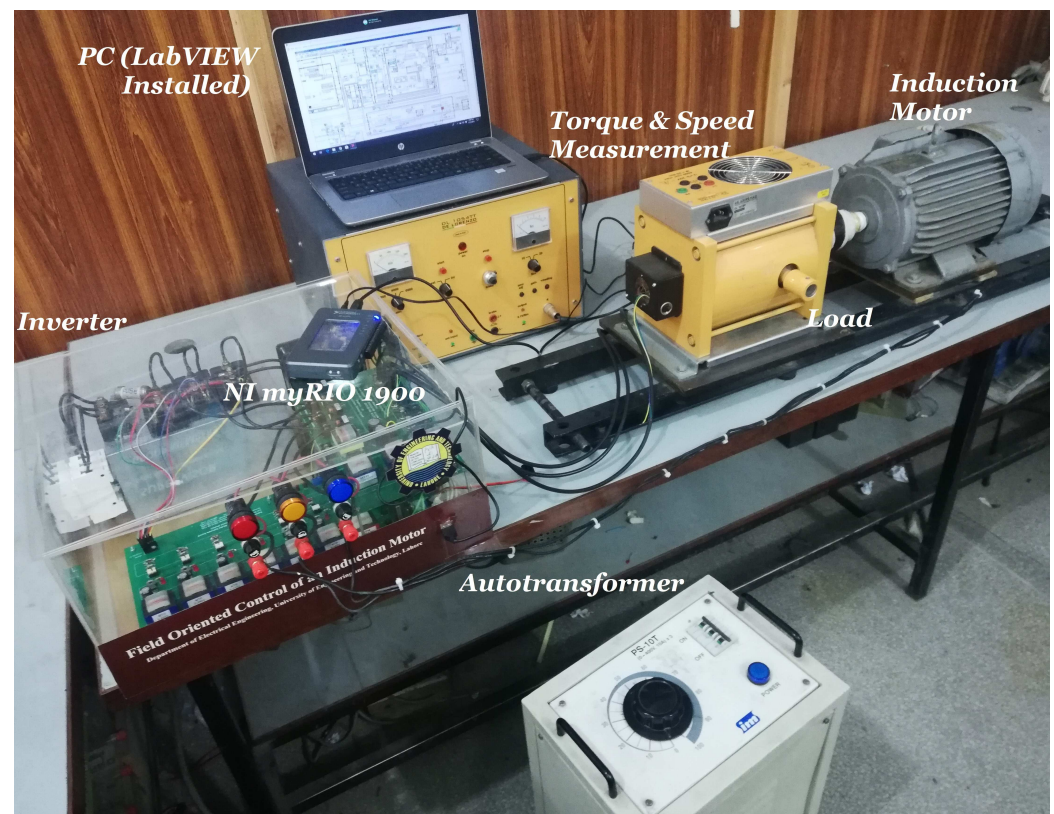

Figure 10. Induction machine drive testing platform.

5.1. HWFET Based Perfomance Analysis

The proposed control scheme is tested against the HWFET driving cycle at an elevated temperature with varying machine parameters (rotor and stator resistance) to ensure that it excellently addresses the conflicting objectives of EV powertrain. To validate its

superiority, its performance is compared with the first-order SMC based FOC technique developed for induction motor control in [32]. The HWFET driving cycle is used as speed profile for testing. The machine parameters are also taken from [32], i.e., $L_M = 41.2$ mH, $r_S = 0.6\,\Omega$, $L_S = 1.9$ mH, $r_R = 0.41\,\Omega$ and $L_R = 1.9$ mH. The obtained results are shown in Figures 11–13.
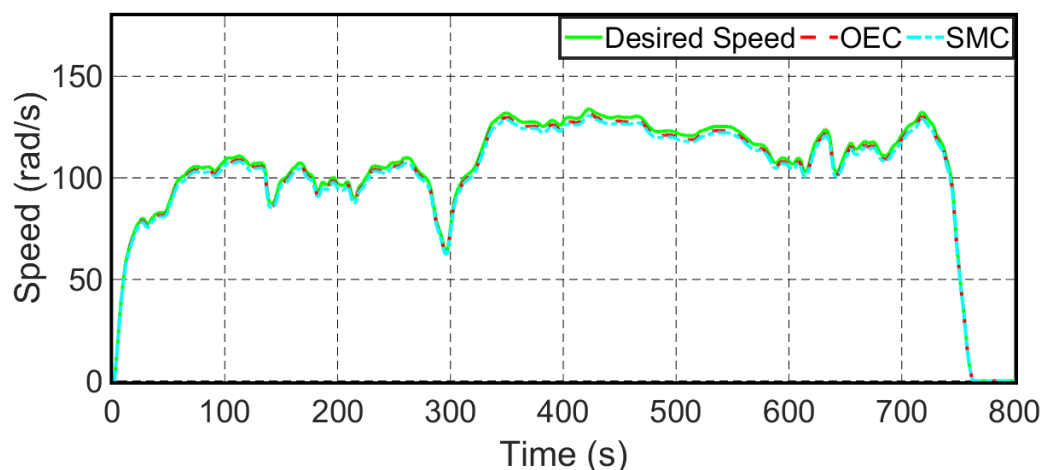

Figure 11. Experimental analysis: HWFET-based analysis at 60 °C.

The accuracy of the proposed OEC is quantitatively assessed to be 99.3%, whereas SMC has 98%, obtained from the speed performance test given in Figure 11. The amplitude of machine drive voltages is of prime importance since it depicts the control effort of the adopted control methodology. Similarly, the amplitude of machine drive currents play a significant role throughout the EV powertrain operation. The greater the amplitudes of these two prime parameters, the greater the drive energy consumption will be that will eventually increase the battery consumption of EV and degrade its performance capability. It can be observed from Figures 12 and 13 that the voltage and current of machine drive in case of OEC scheme are significantly less as compared to that for SMC methodology which validates the reduced drive energy consumption as well as improved working of EV powertrain.
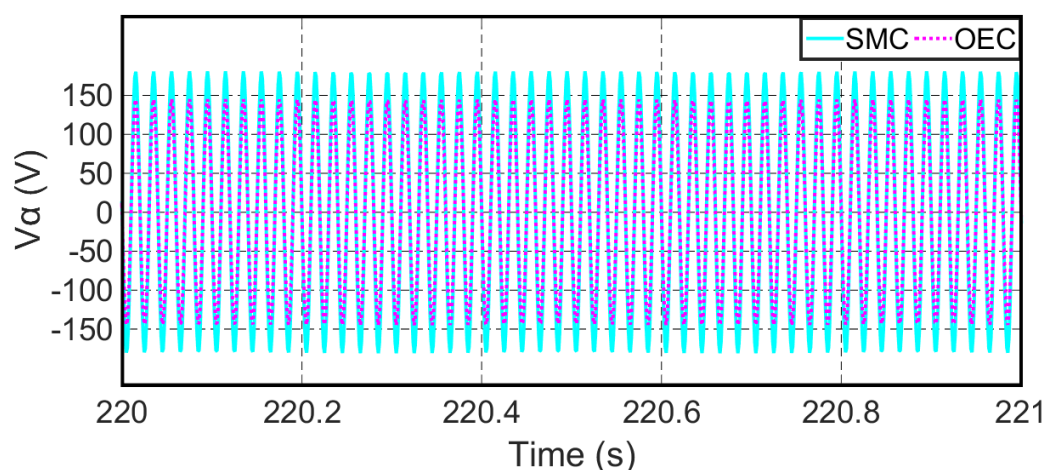

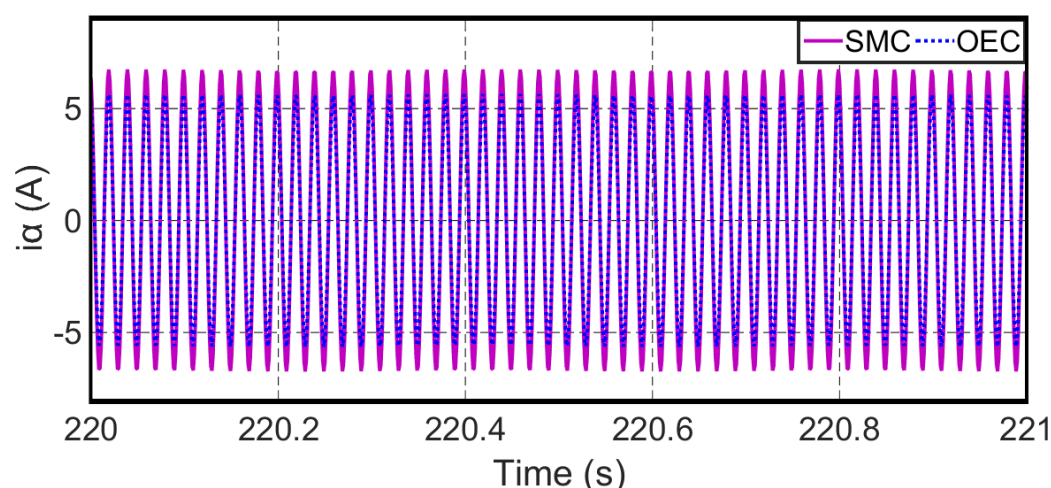**Figure 12.** Experimental analysis: EV powertrain voltages.

Figure 13. Experimental analysis: EV powertrain currents.

5.2. Discussion

As it is a common norm in automotive research, the robustness of a proposed control technique is validated by testing it against various standard driving cycles [5,33]. This test is conducted at an elevated temperature to incorporate the thermal degradation effects on drive performance. The superiority of OEC in comparison with SMC and Higher Order SMC is proved with nonlinear MATLAB-based simulations as well as experimental results. For the simulation section, it can be observed from Figures 6 and 7 that the drive voltages (analogous to the control effort) and the drive currents in case of OEC have a relatively lower amplitude of about 150 volts and 5 amperes, respectively, which shows that relatively lower drive energy is consumed in this case, as compared to its counter control scheme. Furthermore, the better speed tracking performance of OEC is represented by the comparison shown in bar charts of Figure 5 along with percentage variations in stator and rotor resistances. It can be observed that the speed tracking error is significantly low in case of OEC as compared to that in the Higher Order SMC technique. For the experimental section, the same conflicting objectives of maximizing the speed tracking performance and minimizing the drive energy consumption are elaborated for another standard driving cycle. Here, the maximization of speed tracking performance in case of OEC is ensured by its quatitative analysis which comes out to be 99.3% and is higher than that in case of SMC, which is 98%. On the other hand, the drive energy consumption for both types of control techniques is compared by comparing the amplitudes of drive voltage and current. This comparison is shown in Figures 12 and 13, and proves the superioirity of the OEC scheme in efficiently achieving the conflicting objectives.

6. Conclusions

This paper presents an efficient optimized energy control scheme (OEC) for addresing two conflicting objectives of the EV powertrain, which are maximizing its speed performance and minimizing its drive energy consumption. The proposed methodology utilizes an LPV control technique tuned by genetic algorithms to achieve the desired control objectives. To ensure the efficacy of this control scheme, it is compared with other renowned techniques, i.e., SMC and higher order SMC against standard driving cycles (NEDC and HWFET) at elevated temperatures considering the varying machine parameters. The effectiveness of the proposed energy control scheme is validated through simulations as well as experiments. In future, the conflicting objectives of permanent magnet machine drive-based EV powertrain will be addressed by OEC.

Author Contributions: S.M.N.A. conceived, designed and performed the simulation and experimental evaluations and was responsible for preparing the original draft of this paper; M.J.H. and S.C.M. supervised the development of the control scheme and conceptual solution and are responsible for

Abbreviations

The following abbreviations are used in this manuscript:

EV	Electric vehicle
FOC	Field-oriented control
HOSMC	Higher order sliding mode control
HWFET	Highway Fuel Economy Test
LPV	Linear parameter varying
MRAS	Model reference adaptive system
NEDC	New European Driving Cycle
OEC	Optimized energy control
SMC	Sliding mode control

References

1. Chan, C.C.; Bouscayrol, A.; Chen, K. Electric, hybrid, and fuel-cell vehicles: Architectures and modeling. *IEEE Trans. Veh. Technol.* **2009**, *59*, 589–598. [CrossRef]
2. Yu, J.; Pei, W.; Zhang, C. A loss-minimization port-controlled Hamilton scheme of induction motor for electric vehicles. *IEEE/ASME Trans. Mechatronics* **2015**, *20*, 2645–2653. [CrossRef]
3. De Santiago, J.; Bernhoff, H.; Ekergård, B.; Eriksson, S.; Ferhatovic, S.; Waters, R.; Leijon, M. Electrical motor drivelines in commercial all-electric vehicles: A review. *IEEE Trans. Veh. Technol.* **2012**, *61*, 475–484. [CrossRef]
4. Pawlus, W.; Birkeland, J.T.; Van Khang, H.; Hansen, M.R. Identification and experimental validation of an induction motor thermal model for improved drivetrain design. *IEEE Trans. Ind. Appl.* **2017**, *53*, 4288–4297. [CrossRef]
5. Yang, Z.; Shang, F.; Brown, I.P.; Krishnamurthy, M. Comparative study of interior permanent magnet, induction, and switched reluctance motor drives for EV and HEV applications. *IEEE Trans. Transp. Electrif.* **2015**, *1*, 245–254. [CrossRef]
6. Yang, S.; Ding, D.; Li, X.; Xie, Z.; Zhang, X.; Chang, L. A novel online parameter estimation method for indirect field oriented induction motor drives. *IEEE Trans. Energy Convers.* **2017**, *32*, 1562–1573. [CrossRef]
7. De Castro, R.; Araújo, R.E.; Freitas, D. Wheel slip control of EVs based on sliding mode technique with conditional integrators. *IEEE Trans. Ind. Electron.* **2013**, *60*, 3256–3271. [CrossRef]
8. Zhao, L.; Huang, J.; Liu, H.; Li, B.; Kong, W. Second-order sliding-mode observer with online parameter identification for sensorless induction motor drives. *IEEE Trans. Ind. Electron.* **2014**, *61*, 5280–5289. [CrossRef]
9. Marino, R.; Tomei, P.; Verrelli, C.M. A nonlinear tracking control for sensorless induction motors. *Automatica* **2005**, *41*, 1071–1077. [CrossRef]
10. Marino, R.; Tomei, P.; Verrelli, C.M. An adaptive tracking control from current measurements for induction motors with uncertain load torque and rotor resistance. *Automatica* **2008**, *44*, 2593–2599. [CrossRef]
11. Zhou, K.; Doyle, J.C.; Glover, K. *Robust and Optimal Control*; Prentice Hall: Englewood Cliffs, NJ, USA, 1996; Volume 40.
12. Prempain, E.; Postlethwaite, I.; Benchaib, A. A linear parameter variant H∞ control design for an induction motor. *Control Eng. Pract.* **2002**, *10*, 633–644. [CrossRef]
13. Dalila, K.; Abdessalem, M.; Said, D.; Chrifi-Alaoui, L. Robust linear parameter varying induction motor control with polytopic models. *Serbian J. Electr. Eng.* **2013**, *10*, 335–348. [CrossRef]
14. Blanchini, F.; Casagrande, D.; Miani, S.; Viaro, U. An LPV control scheme for induction motors. In Proceedings of the 2012 IEEE 51st IEEE Conference on Decision and Control (CDC), Maui, HI, USA, 10–13 December 2012; pp. 7602–7607.
15. Abdessalem, D.K.; Said, D. Linear parameter varying induction motor control with two-degree-of freedom controller. In Proceedings of the 4th International Conference on Power Engineering, Energy and Electrical Drives, Istanbul, Turkey, 13–17 May 2013; pp. 1748–1752.

16. Salem, A.; Tlili, A.S.; Braiek, N.B. On the polytopic and multimodel state observers of induction motors. *J. Autom. Syst. Eng. (JASE)* **2008**, *2*, 235–247.

17. Farhani, F.; Regaya, C.B.; Zaafouri, A.; Chaari, A. A quasi linear parameter varying approach to robust control of an Induction machine. In Proceedings of the 10th International Multi-Conferences on Systems, Signals & Devices 2013 (SSD13), Hammamet, Tunisia, 18–21 March 2013; pp. 1–5.

18. Khamari, D.; Benlaloui, I.; Ouchen, S.; Makouf, A.; Drid, S.; Alaoui, L.C.; Ouriagli, M. LPV Induction Motor Control with MRAS Speed Estimation. In Proceedings of the 2019 8th International Conference on Systems and Control (ICSC), Marrakesh, Morocco, 23–25 October 2019; pp. 460–464.

19. Krebs, S.; Fugel, S.; Hohmann, S. Interval state observer based on a time-variant transformation for LPV systems and application to induction machines. In Proceedings of the 2017 IEEE Conference on Control Technology and Applications (CCTA), Maui, HI, USA, 27–30 August 2017; pp. 1077–1084.

20. Do, A.L.; Soualmi, B.; de Jesus Lozoya-Santos, J.; Sename, O.; Dugard, L.; Ramirez-Mendoza, R. Optimization of weighting function selection for H∞ control of semi-active suspensions. In Proceedings of the VSDIA 2010-12th Mini Conference on Vehicle System Dynamics, Identification and Anomalies, Budapest, Hungary, 8–10 November 2010.

21. Guazzelli, P.R.U.; de Andrade Pereira, W.C.; de Oliveira, C.M.R.; de Castro, A.G.; de Aguiar, M.L. Weighting factors optimization of predictive torque control of induction motor by multiobjective genetic algorithm. *IEEE Trans. Power Electron.* **2018**, *34*, 6628–6638. [CrossRef]

22. Raj, R.E.; Kamalakannan, C.; Karthigaivel, R. Genetic algorithm-based analysis of wind-driven parallel operated self-excited induction generators supplying isolated loads. *IET Renew. Power Gener.* **2017**, *12*, 472–483. [CrossRef]

23. Ali, S.N.; Hossain, M.; Hanif, A.; Sharma, V.; Kashif, M. A VRC H∞ Design for Dynamic Thermal Derating of Induction Machines. In Proceedings of the 2018 Australasian Universities Power Engineering Conference (AUPEC), Auckland, New Zealand, 27–30 November 2018; pp. 1–6.

24. Ali, S.N.; Hanif, A.; Hossain, M.; Sharma, V. An LPV H∞ Control Design for the Varying Rotor Resistance Effects on the Dynamic Performance of Induction Motors. In Proceedings of the 2018 IEEE 27th International Symposium on Industrial Electronics (ISIE), Cairns, QLD, Australia, 13–15 June 2018; pp. 114–119.

25. Ali, S.N.; Hossain, M.; Sharma, V.; Kashif, M. Tri-Objective LPV Controller Design for the Thermal Management of Motor Drive Parameters in an Electric Vehicle. In Proceedings of the 2020 IEEE Green Technologies Conference (GreenTech), Oklahoma City, OK, USA, 1–3 April 2020; pp. 86–91.

26. Ali, S.N.; Hossain, J.; Wang, D.; Lu, K.; Rasmussen, P.; Sharma, V.; Kashif, M. Robust Sensorless Control Against Thermally Degraded Speed Performance in an IM Drive Based Electric Vehicle. *IEEE Trans. Energy Convers.* **2020**. [CrossRef]

27. Ali, S.N.; Hossain, M.; Sharma, V.; Kashif, M. Thermal Control Compensation of Induction Motor Drive in Electrified Powertrain. In Proceedings of the 2020 IEEE Conference on Technologies for Sustainability (SusTech), Santa Ana, CA, USA, 23–25 April 2020; pp. 1–6.

28. Ali, S.N.; Hanif, A.; Ahmed, Q. Review in thermal effects on the performance of electric motors. In Proceedings of the 2016 International Conference on Intelligent Systems Engineering (ICISE), Islamabad, Pakistan, 15–17 January 2016; pp. 83–88.

29. Zhang, P.; Du, Y.; Habetler, T.G.; Lu, B. A survey of condition monitoring and protection methods for medium-voltage induction motors. *IEEE Trans. Ind. Appl.* **2011**, *47*, 34–46. [CrossRef]

30. Beguenane, R.; Benbouzid, M.E.H. Induction motors thermal monitoring by means of rotor resistance identification. *IEEE Trans. Energy Convers.* **1999**, *14*, 566–570. [CrossRef]

31. Dominguez, J.R.; Mora-Soto, C.; Ortega-Cisneros, S.; Panduro, J.J.R.; Loukianov, A.G. Copper and core loss minimization for induction motors using high-order sliding-mode control. *IEEE Trans. Ind. Electron.* **2012**, *59*, 2877–2889. [CrossRef]

32. Rehman, H.U. Elimination of the stator resistance sensitivity and voltage sensor requirement problems for DFO control of an induction Machine. *IEEE Trans. Ind. Electron.* **2005**, *52*, 263–269. [CrossRef]

33. Williamson, S.S.; Emadi, A.; Rajashekara, K. Comprehensive efficiency modeling of electric traction motor drives for hybrid electric vehicle propulsion applications. *IEEE Trans. Veh. Technol.* **2007**, *56*, 1561–1572. [CrossRef]